


Article

A Drone-Based Structure from Motion Survey, Topographic Data, and Terrestrial Laser Scanning Acquisitions for the Floodgate Gaps Deformation Monitoring of the Modulo Sperimentale Elettromeccanico System (Venice, Italy)

Massimo Fabris *  and Michele Monego 

Department of Civil, Environmental and Architectural Engineering, University of Padua, 35131 Padua, Italy; michele.monego@unipd.it

* Correspondence: massimo.fabris@unipd.it

Abstract: The structural deformation monitoring of civil infrastructures can be performed using different geomatic techniques: topographic measurements with total stations and levels, TLS (terrestrial laser scanning) acquisitions, and drone-based SfM (structure from motion) photogrammetric surveys, among others, can be applied. In this work, these techniques are used for the floodgate gaps and the rubber joints deformation monitoring of the MOSE system (Modulo Sperimentale Elettromeccanico), the civil infrastructure that protects Venice and its lagoon (Italy) from high waters. Since the floodgates are submerged most of the time and cannot be directly measured and monitored using high-precision data, topographic surveys were performed in accessible underwater tunnels. In this way, after the calculation of the coordinates of some reference points, the coordinates of the floodgate corners were estimated knowing the geometric characteristics of the system. A specific activity required the acquisition of the TLS scans of the stairwells in the shoulder structures of the Treporti barrier because many of the reference points fixed on the structures were lost during the placement of elements on the seabed. They were replaced with new points whose coordinates in the project/as-built reference system were calculated by applying the Procrustean algorithm by means of homologous points. The procedure allowed the estimation of the transformation parameters with maximum residuals of less than 2.5 cm, a value in agreement with the approximation of the real concrete structures built. Using the obtained parameters, the coordinates of the new reference points were calculated in the project reference system. Once the 3D orientation of all caissons in the barrier was reconstructed, the widths of the floodgate gaps were estimated and compared with the designed values and over time. The obtained values were validated in the Treporti barrier using a drone-based SfM photogrammetric survey of the eight raised floodgates, starting from the east shoulder caisson. The comparison between floodgate gaps estimated from topographic and TLS surveys, and those obtained from measurements on the 3D photogrammetric model, provided a maximum difference of 1.6 cm.

Keywords: MOSE system; deformations monitoring; drone-based SfM photogrammetry; TLS acquisitions; total station measurements



Citation: Fabris, M.; Monego, M. A Drone-Based Structure from Motion Survey, Topographic Data, and Terrestrial Laser Scanning Acquisitions for the Floodgate Gaps Deformation Monitoring of the Modulo Sperimentale Elettromeccanico System (Venice, Italy). *Drones* **2024**, *8*, 598. <https://doi.org/10.3390/drones8100598>

Academic Editors: Eben N. Broadbent and David R. Green

Received: 10 September 2024

Revised: 10 October 2024

Accepted: 16 October 2024

Published: 18 October 2024



Copyright: © 2024 by the authors. Licensee MDPI, Basel, Switzerland. This article is an open access article distributed under the terms and conditions of the Creative Commons Attribution (CC BY) license (<https://creativecommons.org/licenses/by/4.0/>).

1. Introduction

Geomatic techniques have proven to provide very useful data in the monitoring of deformations [1]. Their integration allows improving the information, overcoming the characteristic limits of each methodology, and in many cases, providing an estimation of the data accuracies [2,3]. The deformations monitoring of civil structures and infrastructures requires high precision measurements that are repeated over time and co-registered in the same reference system. The deformation of infrastructures like bridges, dams, railways, historical buildings, expressways, etc., are commonly monitored using total stations [4,5]

that can be integrated with TLS (terrestrial laser scanning) [6], photogrammetry [7], GNSS (global navigation satellite system) [8,9], and InSAR (interferometric synthetic aperture radar) [10].

The instruments can be fixed on the structures and/or mounted on different platforms, but the use of UAV (unmanned aerial vehicle) systems is, in most cases, the most efficient option to reach the inaccessible portions of the objects, providing a complete coverage of the infrastructure to be monitored [11]. In the literature, many works about aerial photogrammetry with drones used for the multi-temporal monitoring of civil infrastructures (both during construction and subsequent maintenance) can be found. Applications are related to structural damage assessments after disasters [12], the monitoring of aging buildings and dams [13], crack detection in buildings [14], concrete crack identification [15,16], crack detection in bridges [17], the inspection and quantification of bridge deterioration [18,19], the detection of crack patterns in historical structures [20], the measurement and monitoring of concrete structures [21], buildings inspection and structural health monitoring [22,23], road infrastructure construction sites monitoring [24], construction site surveillance and monitoring [25,26], the maintenance of railway infrastructure [27], and many others.

Data obtained from drone-based photogrammetry and ground-based total station and level are comparable, and differences of a few centimeters can be obtained [28]. For this reason, the two techniques can be integrated for deformation monitoring applications [29]. Varbla et al. [30] used UAV-based photogrammetry in the survey of the 150 m long Tallinn–Tartu highway (Estonia). The 3D model, extracted to estimate the road structure deformations, was compared with ground-based high-precision leveling data obtaining an RMSE (root mean square error) of less than 1 cm, showing that UAV photogrammetry can be used for the centimeter-range deformation monitoring of the built environment. Zrinjski et al. [31] compared the UAV-based photogrammetric approach with data obtained using a total station for the structural analysis of the chimney and determination of the inclination in a high industrial masonry chimney located in Duga Resa, Croatia. The authors obtained better results by the total station-based surveys, while they recommended great attention to the accuracy of the UAV-generated point cloud if high precision is needed. Adi et al. [32] compared the measurements of the total station with those obtained from UAV-based photogrammetry in a railway infrastructure monitoring system. The authors surveyed a 1 km long railway track located in the Indonesian Railway Polytechnics Madiun Laboratory, Madiun, East Java. The results showed no statistical differences between the two datasets.

In this work, the drone-based photogrammetric technique was used together with total station measurements to monitor the floodgate gaps of the MOSE system (Modulo Sperimentale Elettromeccanico), the mobile gates system that protects Venice and its lagoon (Italy) from high waters (Figure 1).

The monitoring of this infrastructure presents different peculiar challenges, in terms of both technical solutions and environmental difficulties. The complexity of the whole structure (submerged and emerged portions with narrow connection tunnels, mobile elements, shafts, and stairs), require robust topographic procedures and data acquisition in order to obtain reliable measurements with adequate accuracies. An overall error on the order of 1 cm is the constraint value that allows an acceptable application of the survey methods in order to evaluate the integrity of the monitored parts and the functionality of the mobile floodgates both during the raising and lowering phases. The integration between topographic and 3D data allows for further analysis, such as the spatial positioning of some elements of the structure, to detect reliable differential displacements.

1.1. The MOSE System

1.1.1. Characteristics of the System

The mobile gate system, the experimental electromechanical module (MOSE), was planned to temporarily isolate the Venetian lagoon from the Adriatic Sea during high waters and severe storm surge events [33]. It is composed of four barriers located in the

inlets of Chioggia, Malamocco, and Lido (the latter subdivided in the San Nicolò and Treporti inlets by an artificial island) that defend the city of Venice and its lagoon (Figure 2).

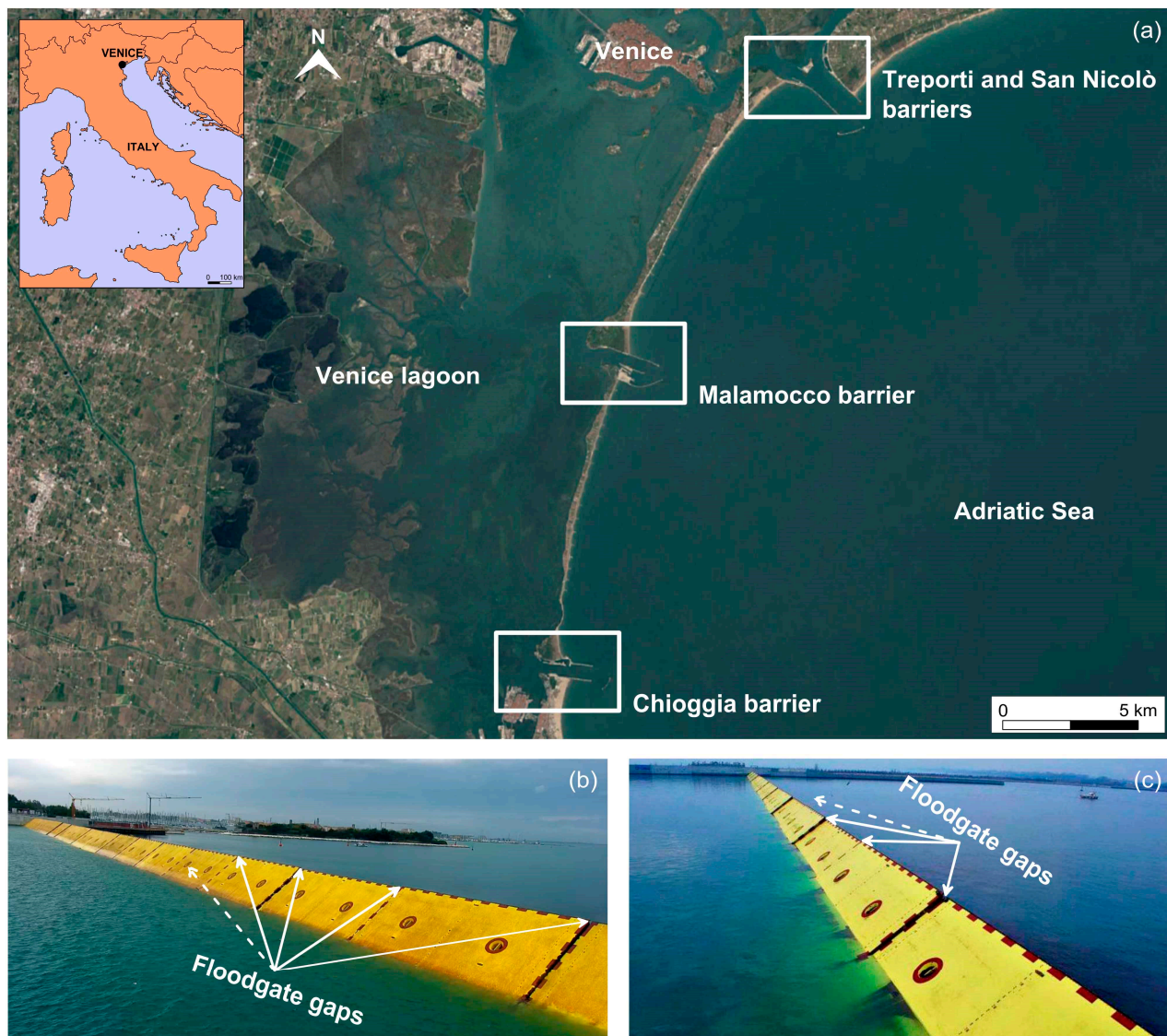


Figure 1. Location of the four barriers (in many works, Treporti and San Nicolò are included in the Lido barrier) that identify the mobile dam system (MOSE—Modulo Sperimentale Elettromeccanico—system) that protects the city of Venice and its lagoon from high waters (a). Metallic floodgates (in yellow) ((b,c) edited from Consorzio Venezia Nuova website) are embedded in concrete caissons, placed 20 to 25 m below the mean sea level, and are raised during high-water events. The floodgate gaps are indicated (b,c): monitoring is necessary to avoid contact and collisions during the handling and operational phases.

The construction started in 2003 and is now in the completion phase. In each lagoon barrier, concrete lodging caissons, located along the development of the inlet, were built on construction sites and placed on the seabed [34]. The first and last caissons, placed in the two lateral areas (the shoulder caissons), are characterized by emerged structures, while the others are completely submerged.

The number of caissons and the submerged depth change in each barrier due to the different lengths (from 370 to 450 m), and depths (in the range from 6 m to 20 m) had to be covered. The caissons, with dimensions of 59.2 m, 36.2 m, and 8.7 m, longitudinally to the barrier, perpendicularly, and vertically, respectively (in the Treporti barrier), were

placed on pile foundations to increase their stability. They were connected to each other by means of main and secondary tunnels, which can be reached via the stairwells from the emerged structures of the two shoulder caissons. Along the tunnels, between the adjacent caissons, rubber joints were planned and fixed at the structures' borders to protect the tunnels against flooding. Subsequently, on each caisson, three metallic floodgates were lodging with dimensions of 19.88 m, 19.34 m, and 3.6 m, longitudinally to the barrier, perpendicularly, and vertically, respectively (in the Treporti barrier). They are characterized by gaps of 12 cm for the metallic elements belonging to the same caisson, and 20 cm for the floodgates belonging to adjacent caissons (these values are the measure of the gaps defined in the project, as reported in Figure 3). To cover the length of each barrier, 21, 20, 19, and 18 floodgates were necessary at the Treporti, San Nicolò, Malamocco, and Chioggia inlets, respectively [35].

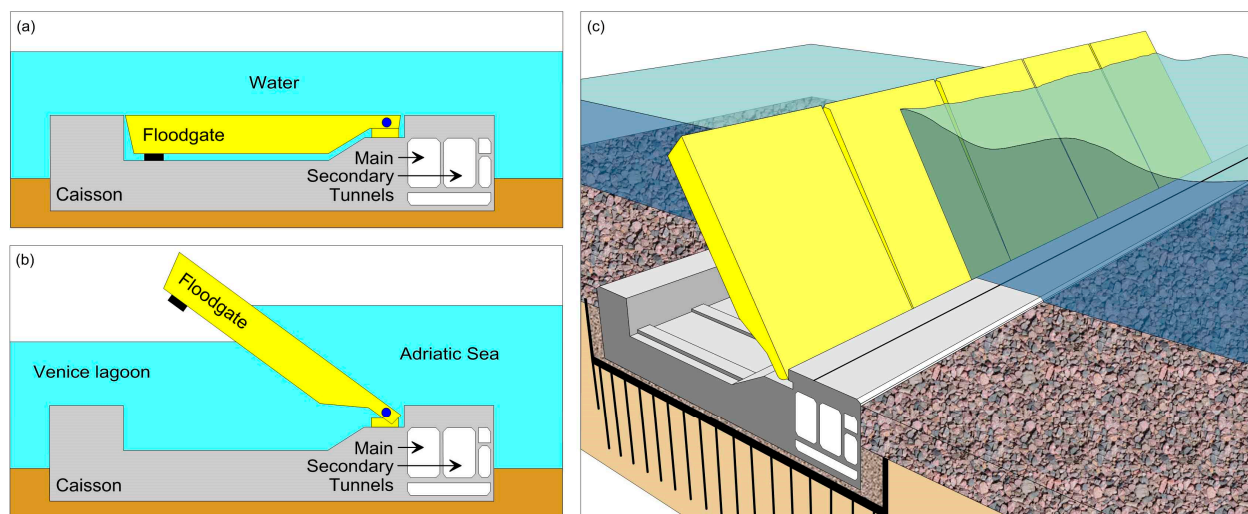


Figure 2. Operating phases of the MOSE system: (a) metallic floodgate housed in the concrete caisson; (b) floodgate raised during high waters; (c) scheme representing a 3D view of the system during operation.

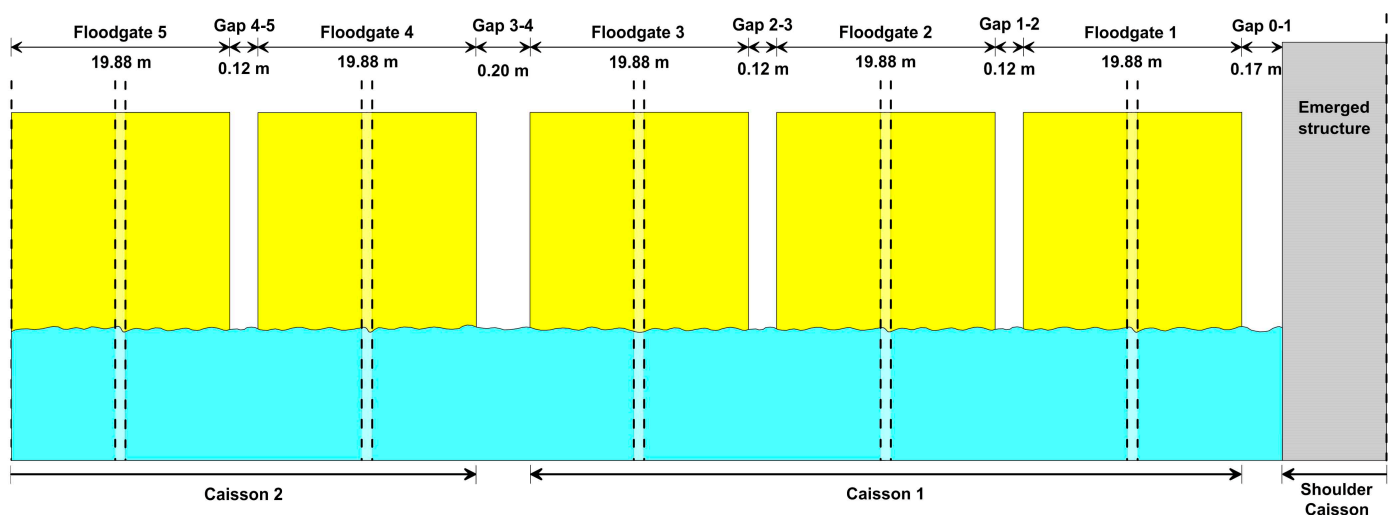


Figure 3. Values of the designed floodgate gaps: 0.17 m between the shoulder and the first floodgate of the first caissons, 0.12 m between the floodgates housed in the same caisson, and 0.20 m between the floodgates belonging to adjacent caissons. The longitudinal size of the raised floodgates (in yellow, three per caisson) is also reported. The shoulder caisson is characterized by emerged structures (in gray). The light blue indicates the seawater.

The floodgates are raised when the forecasted water level is higher than a safeguarding value that normally is set to 110 cm, because in this case, most of the pavements of the historical city of Venice are reached by water [36]. In the first 29 months of test operations, from October 2020, the system came into operation 44 times, about 20 times per year, with a rate 10 times higher than expected [37].

1.1.2. Rubber Joints and Floodgate Gaps Monitoring

One of the most critical elements of the system are the rubber joints that connect the concrete lodging caissons located on the seabed. They are essential for the protection of the main and secondary tunnels. In conjunction between two subsequent caissons, the rubber joints are characterized by two components: the first is directly in contact with the seawater and the second is directly visible in the tunnels (Figure 4).

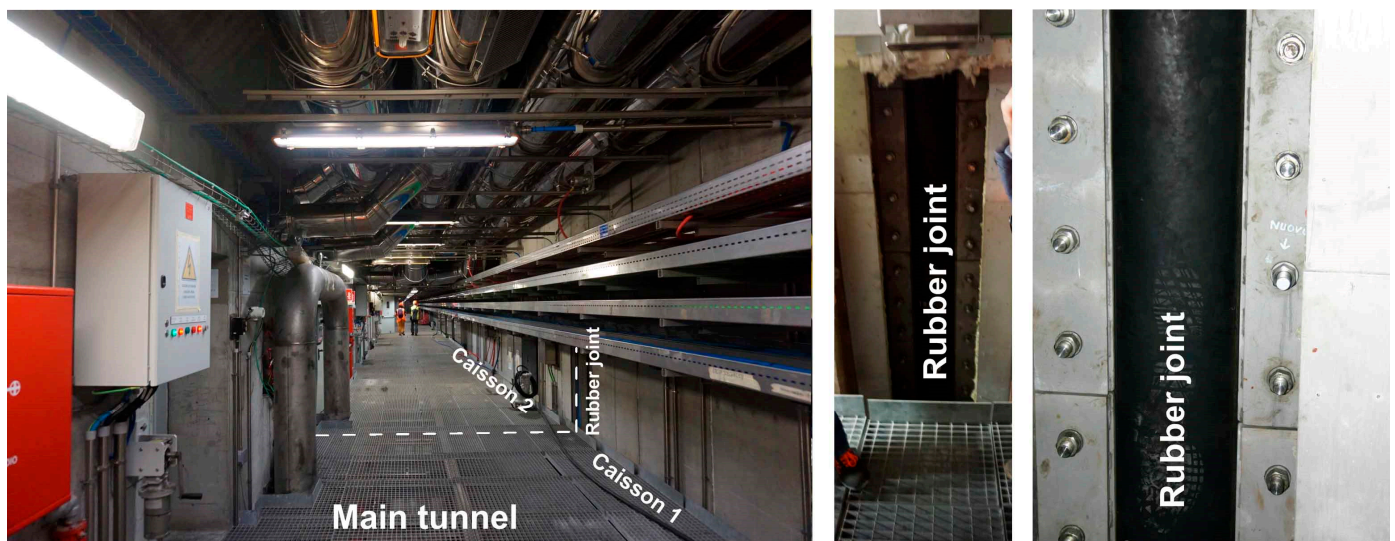


Figure 4. Rubber joints that protect the main and secondary tunnels from flooding along the separation between the subsequent caissons.

Due to the limited flexibility of the rubber joints, the 3D relative displacements between the caissons could damage these fragile elements, leading to collapse and the consequent flooding of the tunnels. For this reason, the monitoring of the relative deformations of the caissons is crucial for assessing the correct functionality of the joints and the protection of the tunnels and operators during work activities (Figures 4 and 5).



Figure 5. Scheme representing the tunnels that connect the concrete caissons and are protected against flooding by the rubber joints. The shoulder caissons are characterized by emerged structures, whereas the caissons that host the floodgates are submerged and located on the seabed.

From the beginning of construction, the deformation monitoring of these submerged elements was then performed using a total station: (i) starting from stable points fixed outside to the structures; (ii) measuring the coordinates of reference points located along the tunnels, belonging to the different caissons; (iii) and comparing the multi-temporal data with the threshold values to assess the risk level.

The second critical element of the system that requires accurate deformations monitoring of the caissons is the floodgate gap. Due to each caisson containing three floodgates,

the most important analysis is related to the deformations monitoring of the gaps between floodgates located in the subsequent caissons. The relative deformation of the caissons could generate collisions during both the raising of the floodgates (Figure 3) and their operations. Accurate monitoring is essential. For this reason, because the floodgates are submerged most of the time and the corners cannot be directly measured with high precision using geomatic techniques, the monitoring system was implemented by using total stations and measuring benchmarks located in the tunnels and belonging to the different caissons. Subsequently, knowing the geometries of the system, the coordinates and the distances between the floodgate corners are calculated and compared both with the designed values and over time, to evaluate the safety level against possible collisions. However, this method is penalized by the unfavorable geometry of the structure as measurements with the total station are limited to the tunnels (Figure 2a,b). For this reason, a different approach, based on structure from motion (SfM) photogrammetry with images acquired by a drone of the raised floodgates, was tested. In this way, the values calculated using the topographic measurements can be validated. During the image acquisition, it is essential that there are no moving elements; for this reason, particular attention must be paid during the survey because the wave motion could cause a movement of the floodgates.

1.2. Objectives of the Work

The aim of this work is to evaluate the efficiency and accuracy of topographic measurements using total stations and levels in MOSE system tunnels for the definition and monitoring of rubber joints and floodgate gap dimensions. For each (topographic) survey, a 3D spatial positioning of each caisson and the distances between the floodgates (and, of course, the rubber joints displacements) are calculated. Subsequently, the obtained values are compared with the following: (i) the measurements performed on a 3D SfM photogrammetric model extracted from a survey performed with a drone on the raised floodgates in the Treporti barrier to evaluate the accuracies; and (ii) the designed values and the multi-temporal acquisitions to estimate the deformations over time.

A specific study was carried out for the shoulder caissons in the Treporti barrier because the ‘as built’ reference points, located in the structures during the building on the construction site, were damaged and lost during the placement of the caissons in the barrier. Consequently, the relative displacements between the shoulders and the adjacent caissons of the barrier cannot be evaluated after the location of the elements on site. For this reason, new reference points were fixed on the structures after placement. To calculate their coordinates in the project reference system (crucial for the calculation of the multi-temporal 3D orientations of the shoulder caissons), TLS surveys of the stairwells were performed in order to obtain points with double coordinates (both in project and survey reference systems), necessary for the calculation of the transformation parameters. In this way, the coordinates of the new reference points can be obtained in the project reference system, allowing the definition of the 3D spatial positioning of the shoulder caissons with respect to the designed 3D values. With these data and those related to the references in all the caissons, the 3D spatial orientation of the barrier can be calculated for each survey, allowing the rubber joints and floodgate gap deformations to be monitored. Figure 6 shows the flowchart of this work.

Compared with the above-mentioned works, the floodgate gap monitoring of the MOSE system is a further challenge, both for the surveys with a total station (because the structures are mostly submerged and data can be acquired only in the tunnels) and the drone-based SfM photogrammetry (because when the floodgates are raised, their stability in time is not guaranteed due to the sea wave motion).

In addition, the deformations monitoring of underground/submerged infrastructures, susceptible to high flood risk [38], is a challenge because high precision geomatic measurements cannot be directly applied.

This work is organized as follows. Section 2 describes the surveys performed using the different techniques, the procedures adopted in the processing and calculation of the

floodgate gaps, and the approaches used in the comparisons. Section 3 provides and discusses the obtained results focusing on floodgate gap validation and deformations monitoring, and Section 4 summarizes the work and provides some conclusions.

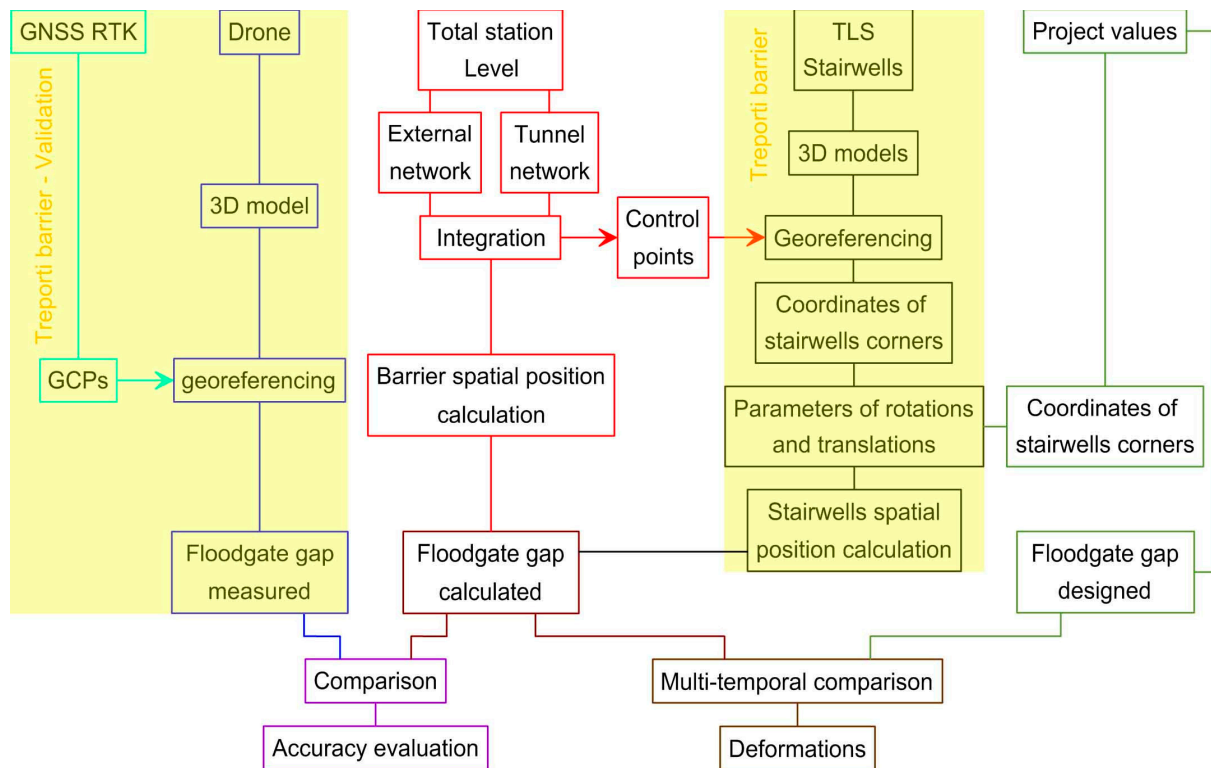


Figure 6. The flowchart of this work.

2. Materials and Methods

2.1. Topographic Surveys

Topographic surveys were conducted repeatedly during the construction of the structures, the placement of the caissons in the barriers, and subsequently, for the deformation monitoring. Angle and distance measurements were executed using total stations with accuracies of $0.5''$ for angles and $1 \text{ mm} + 1 \text{ ppm}$ for distances starting from stable points fixed outside the construction site area. In all barriers, external networks were implemented with benchmarks located on the emerged structures and surrounding areas and internal networks in the main and secondary tunnels; in these compartments, the benchmarks were located in the different caissons, extending as much as possible the surfaces enclosed by the points and adding redundant references at the edges of each caisson. The internal and external networks were connected by means of the vertical open space (vertical shafts) and the stairwells located on the shoulder caissons. Each survey was planned and executed with overabundant measurements, allowing the subsequent adjustment of the networks. Surveys operations, even if different for the four barriers because they were constructed by different companies (different schemes of the networks, different instruments, and procedures), were repeated over time by using the same approaches. Each time, the coordinates of the points located outside of the construction site area were fixed, and the coordinates of the points located on the MOSE structures were calculated and compared to analyze the 3D displacements. Over time, but especially during the first construction phases, many benchmarks were lost due to the interaction of the survey operations with many other different activities and operators that worked simultaneously. The consequence was the replacement of these points with new benchmarks. For this reason, the trend of deformation over time was discontinuous and not was guaranteed for many points. Together, with the topographic surveys using total stations, the geometric leveling technique was applied for accurate

elevation measurements. Multi-temporal leveling lines were performed with the same procedure: (i) starting from stable points outside the construction site area; (ii) measuring many points of the external topographic network; (iii) following the stairwell to reach the tunnels; (iv) measuring many points of the internal network in the main and secondary tunnels with benchmarks located on the subsequent caissons; (v) rising from the submerged surfaces following the other side of the barrier by using the stairwell; and (vi) closing the measurements on other stable points outside to the construction site area. The surveys were carried out with high frequency during the construction period, while, at the present, with the achieved consolidation of the structures, the four barrier measurements are carried out each 6/12 months. As an example, the surveys conducted on 21 March 2023 in the Treporti barrier and 1 June 2023 in the Malamocco barrier provided the data summarized in Table 1. Surveys were carried out by the TE.MA company (Te.Ma.snc, Faenza, Ravenna—Italy) and were commissioned by the Consorzio Venezia Nuova, the agency that manages the mobile dam system.

Table 1. Numbers that summarized the topographic measurements using the Leica Nova TS60 (Leica Geosystems AG, Heerbrugg, Switzerland) total station performed on 21 March and 1 June 2023 in the Treporti and Malamocco barriers, respectively. The numbers of points, stations, distances, angles, trigonometric differences in elevation, and the redundancy of the networks, separated for the barriers, for external and internal networks, and horizontal and vertical processing are highlighted.

Barrier	Network	Horizontal				Vertical		
		Points	Stations	Distances and Angles	Redundancy	Points	Trigonometric Differences in Elevation	Redundancy
Treporti	External	59	15	95	75	59	95	37
	Internal	129	18	243	231	129	243	115
Malamocco	External	42	11	85	89	42	85	44
	Internal	101	16	226	253	101	226	126

Subsequently, for each survey in each barrier, separately for external and internal, and horizontal and vertical networks, data were adjusted using different software (Leica Infinity version 4.0.0.44003, GeoMax Positioning X-Pad version 2023), calculating the 2D and 1D coordinates of the points and the associated uncertainties. The obtained results by the TE.MA. company were checked by the authors using Infinity software. In Table 2, as an example, the mean and RMSE (root mean square error) values of the differences between the obtained coordinates, both for the Treporti and Malamocco barriers, are reported.

Table 2. Mean and RMSE (root mean square error) values of the differences between the coordinates of the points related to the external and internal networks in the Treporti and Malamocco barriers calculated in this study and obtained by the TE.MA. company.

Barrier	Network	Differences in Coordinates: This Study—TE.MA Company		
		East (m)	North (m)	Elevation (m)
Treporti	External	0.0027 ± 0.0003	0.0017 ± 0.0002	0.0010 ± 0.0002
	Internal	0.0006 ± 0.0000	0.0042 ± 0.0003	0.0005 ± 0.0000
Malamocco	External	0.0009 ± 0.0001	0.0007 ± 0.0001	0.0019 ± 0.0002
	Internal	0.0023 ± 0.0002	0.0008 ± 0.0001	0.0027 ± 0.0002

The differences reported in Table 2, on the order of a few millimeters, are in agreement with the expected accuracies using total stations when networks composed of tens of points are analyzed and many measurements are performed [5,10].

From the obtained coordinates, for each survey, the coordinates of the floodgate corners were calculated on the basis of the designed geometrical characteristics of the

structures. Subsequently, the gaps between the adjacent metallic elements, as well as the distances between the adjacent caissons, were calculated and compared with the designed values and over time for the rubber joints and floodgate gaps deformation monitoring.

Together with topographic measurements, a specific 3D TLS survey needs to be conducted in the Treporti barrier.

2.2. TLS Surveys for the 3D Orientation of the Shoulder Caissons in the Treporti Barrier

A specific detailed study required the calculation of the 3D spatial orientation of the shoulder caissons in the Treporti barrier. This was necessary because most of the project reference points, fixed in the structures during construction, were lost during the work activities for the installation of the caissons. The consequence was the impossibility of calculating the following: (i) the multi-temporal 3D relative positioning of the shoulder structures during their operation; (ii) the floodgate gap between the shoulder structure and the first floodgate of the barrier; and (iii) the rubber joint deformations monitoring between the shoulder and the first caissons of the barrier. To solve the problem, new reference points were fixed on the shoulder structures after the placement of the caissons on the seabed. However, their coordinates, which were measurable in the survey reference system, were unknown in the project reference system. The transformation parameters between the two references, necessary to calculate the as-built coordinates, were estimated using homologous points between the project/as-built elements (the designed shoulder caissons) and the real structures in the barrier (and the real position in the barrier). In detail, for each shoulder caisson, the corners of the stairwells and the vertical shafts (the most suitable elements, among those available, to be easily identified in the project) were identified. The coordinates of these points in the project reference system were defined using AutoCAD software version 2021. The calculation of the homologous coordinates (in the survey reference system) of the real structures located in the barrier was carried out by means of a 3D survey of the stairwells and the vertical shafts. In this way, using the double coordinates, the transformation parameters (rotations and translations) between the two reference systems were calculated applying the Procrustean algorithm [39,40]. Subsequently, the coordinates of the new points in the project reference system were calculated applying the parameters of rotations and translations previously obtained; in this way, the subsequent monitoring activities can continue using these new reference points.

Direct survey of the stairwells and vertical shafts corners using a total station was considered unsuitable due to the presence of rounded corners and, in general, for the irregularities that characterized the real-built structures. The TLS survey was preferable to extract the coordinates of the corners in the survey reference system. Surveys were conducted in July and September 2023 for the east and west stairwells and vertical shafts, respectively, using a Leica HDS7000 (Leica Geosystems AG, Heerbrugg, Switzerland) laser scanner and the Leica Nova TS60 (Leica Geosystems AG, Heerbrugg, Switzerland) total station. The station was necessary for the survey of the reference polygonal along the stairwells and the measurements of control points used for the alignment of the acquired scans (the polygonal started and ended on points of the reference networks). The surveys were performed by the TE.MA company, acquiring 16 scans with a mean density of 5 mm, both for the east and west structural elements. Unfortunately, the 3D surveys of the vertical shafts were performed with unfavorable geometries due to the limited available spaces for the stationing of the instrument. During the surveys, five other specific points were measured with the total station, both in the east and west shoulder caissons. They were located close to the rubber joint of separation between the shoulders and the adjacent caissons in the main tunnel. The coordinates of these new points, which were not directly visible, were calculated in the survey reference system from the measurements according to well-defined horizontal and vertical planes; on the contrary, the coordinates of the homologous points in the projects/as-built reference system were easily obtained from the CAD data.

Concerning the mobile structures (floodgates), the SfM drone-based photogrammetric survey was necessary to co-validate the topographic and TLS data.

2.3. SfM Photogrammetric Drone-Based Survey of the Raised Floodgates in the Treporti Barrier

The SfM drone-based photogrammetric survey of the raised floodgates in the Treporti barrier was performed on 11 April 2023 by the TE.MA company. A DJI Phantom 4 pro 2.0 PPK photogrammetric drone equipped with a 20 Megapixel camera was used for image acquisition. The photogrammetric survey involved the system composed of the emerged structures of the east shoulder caisson and the first eight floodgates raised for scheduled maintenance operations. The flight was carried out with a relative altitude of about 30 m and zenithal acquisitions of the camera; the resulting GSD (ground sample distance) was about 5 mm/px. A regular grid geometry with adequate overlap between images was used that guaranteed the coverage of at least 9 photos for every point of the surveyed area. During the survey, the lighting was uniform enough, avoiding significant shadow area in the images. There was an absence of wind and sea wave motion, which guaranteed the stability of the raised floodgates. Overall, 100 images were acquired. Furthermore, 14 natural GCPs (ground control points), well recognizable on site, were chosen and measured on the emerged structures of the east shoulder using the GNSS RTK (real-time kinematic) technique. In this way, the real-time co-registration of the photogrammetric information in the UTM (universal transverse mercator) reference system can be improved and checked with the post-processing of the acquired data. For the production of the point cloud, the processing of the images was performed using Agisoft Metashape software version 1.8.4 [41,42], using both the GCPs and the image center of acquisitions. In detail, the GCPs were subdivided in control points (CPs, 10) used in the processing, and check points (ChPs, 4) used to evaluate the precision of the extracted 3D model [43,44] (Figure 7).

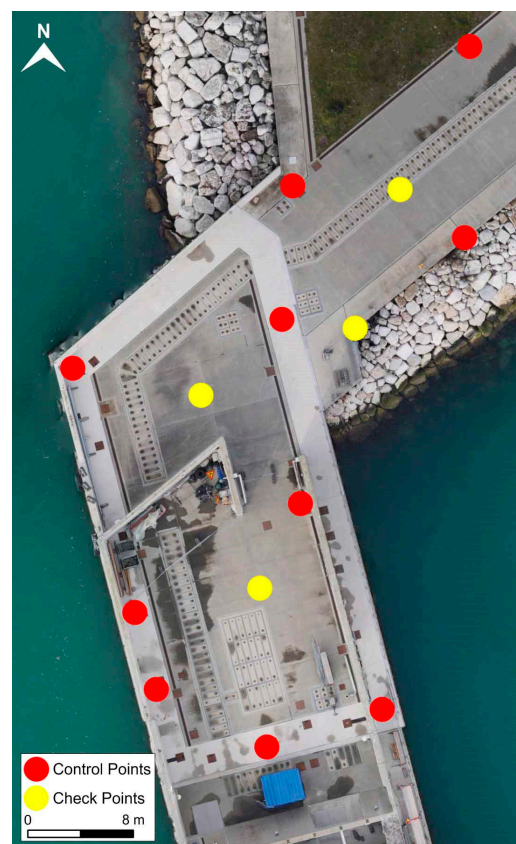


Figure 7. Location of the 10 control points (CPs, used in the processing) and the 4 check points (ChPs, used to evaluate the precision of the extracted 3D point cloud) on the emerged structures of the east shoulder caisson of the Treporti barrier and the surrounding area.

3. Results and Discussion

3.1. The 3D Orientation of the Shoulder Caissons in the Treporti Barrier

The alignment of the acquired point clouds was performed using Cyclone Register 360 plus software version 2023.1.0 [44,45]. In the first phase, the scans were co-registered using the cloud-to-cloud method, obtaining an error of 3 mm, both for the east and west stairwells. In the second phase, the 3D models were co-registered in the survey reference system using the coordinates of the control points extracted from the polygonal measured with the total station. Finally, mean errors within 5 mm were obtained (Figure 8). These values are in agreement with those obtained by other authors in similar studies [46,47].

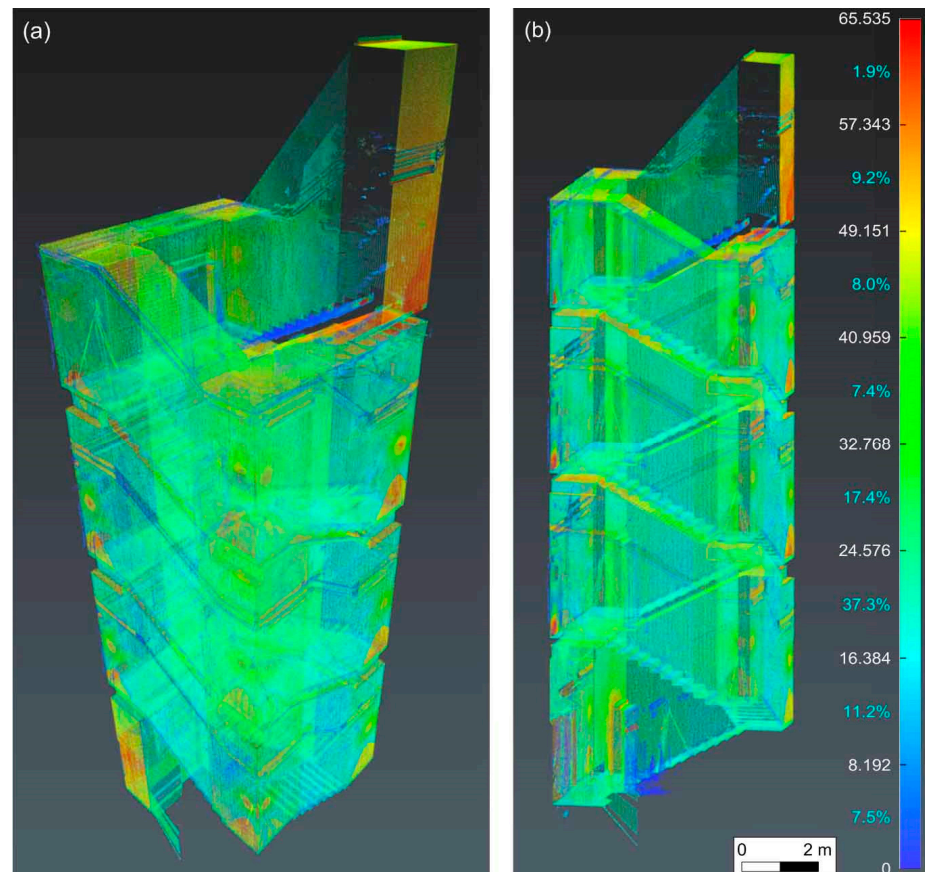


Figure 8. 3D point cloud model representing the east shoulder caisson stairwell in the Treporti barrier; perspective view (a) and orthogonal projection (b) with a color scale based on reflectivity values.

Subsequently, for each point cloud of the stairwells, six approximating planes (floor, ceiling, and the four lateral walls) were extracted using CloudCompare software version 2.12 alpha [48] (Figure 9).

The RMS errors of the results on the order of a few millimeters are shown in Table 3.

Table 3. Approximation of the final 3D point clouds with planes. Results are provided in terms of RMS for the stairwells of the east and west shoulder caissons in the Treporti barrier and separately for each plane: the floor, the four lateral walls, and the ceiling.

Stairwell	Floor (mm)	Lateral Walls				Ceiling (mm)
		1 (mm)	2 (mm)	3 (mm)	4 (mm)	
East	3.1	5.1	3.1	5.2	3.6	4.2
West	2.3	3.8	5.4	3.5	4.9	4.4

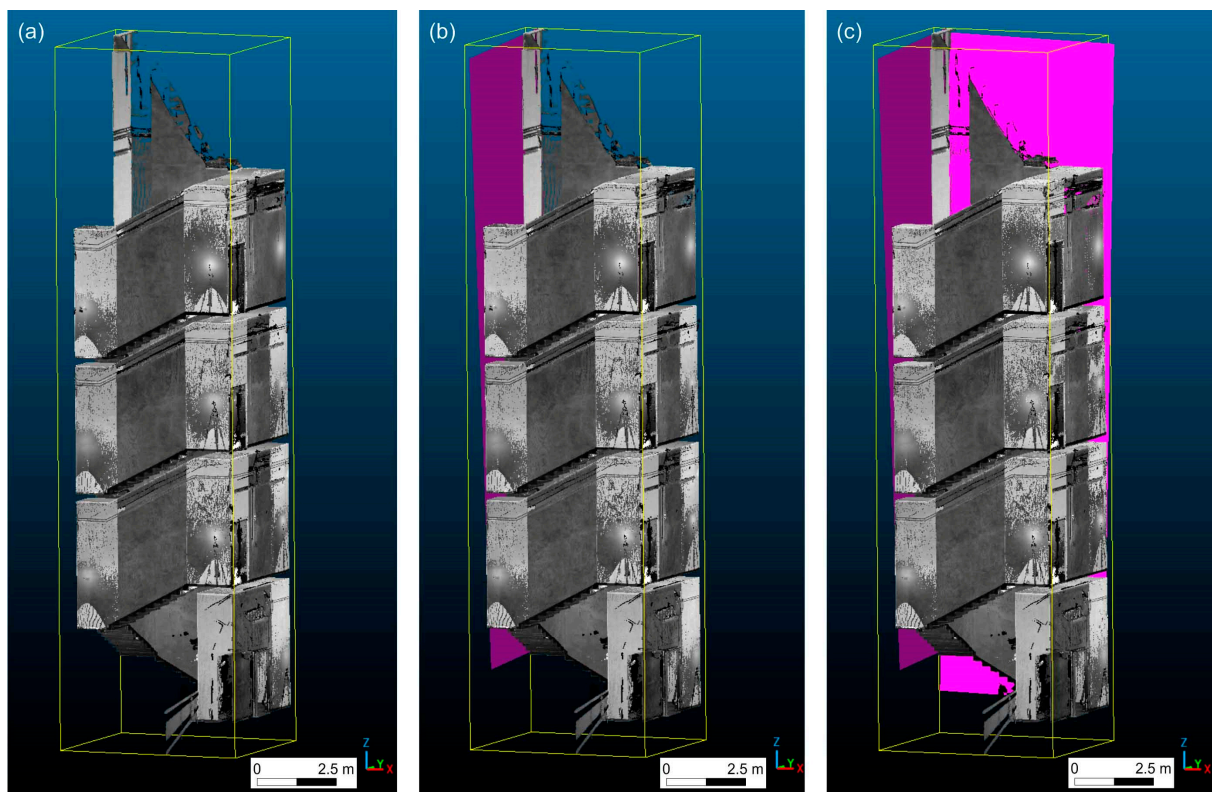


Figure 9. 3D point cloud model (reflectivity in gray values) representing the west stairwell (a) and two of the approximating planes (lateral walls, (b,c), in purple).

The results in Table 3 show values that agree with the irregularities of the real walls constructed and the accuracies of the laser scanner used. Finally, the coordinates of the eight corners of the surveyed stairwells in the survey reference system were obtained by the intersection between these interpolating planes.

The same procedure, applied to the point clouds of the vertical shafts, allowed to obtain the coordinates of the four upper corners in the survey reference system (due to the walking gratings and subservices that covered the lower portion of the walls and the floor, the coordinates of the four lower corners were not calculated). In the transformation procedure, for the calculation of the rotation and translation parameters between the project/as-built and the survey reference systems, for each shoulder caisson that was considered, the following were used: (i) the eight corners of the stairwell and the four corners of the shaft; (ii) the five points directly measured with the total station in the main tunnel between the shoulder and the first caissons of the barrier (recognized in the project and, therefore, with known coordinates in the project reference system); and (iii) the other four points related to the corners of the shoulder caisson plate to improve the geometry of calculation (Figure 10).

The coordinates of these additional points were defined from the project, while the coordinates in the survey reference system were obtained as follows: (i) from the complete survey from 2015 for the planimetric components (given the absence of horizontal displacements in the analyzed period); and (ii) from the same survey from 2015, applying a settlement obtained from the comparison between the elevation surveyed in March 2023 on other points and the elevation of the homologous points surveyed in 2015 for the vertical component, assuming the non-deformable structures.

Subsequently, the study was conducted using the 6-parameter rigid transformation applying the Procrustean algorithm on the MATLAB programming platform, and using the double coordinates of points described above as input data. A first analysis suggested to exclude the four corners of the vertical shaft compartment, both for the east and west shoul-

der caissons, because in the transformation procedure, these points provided a residual greater than 3 cm (maximum values). This result was due to the unfavorable acquisition geometries of the scans in the vertical shafts compared to those of the stairwells, with consequent greater difficulty in extracting the coordinates of the corners in the survey reference system. For this reason, both for the east and west shoulder structures that were considered, the following were used: (i) the eight corners of the stairwell, (ii) the four corners of the shoulder caisson plate, and (iii) the five points located close to the rubber joint of the separation between the shoulder and first caissons of the barrier in the main tunnel (Figure 10).

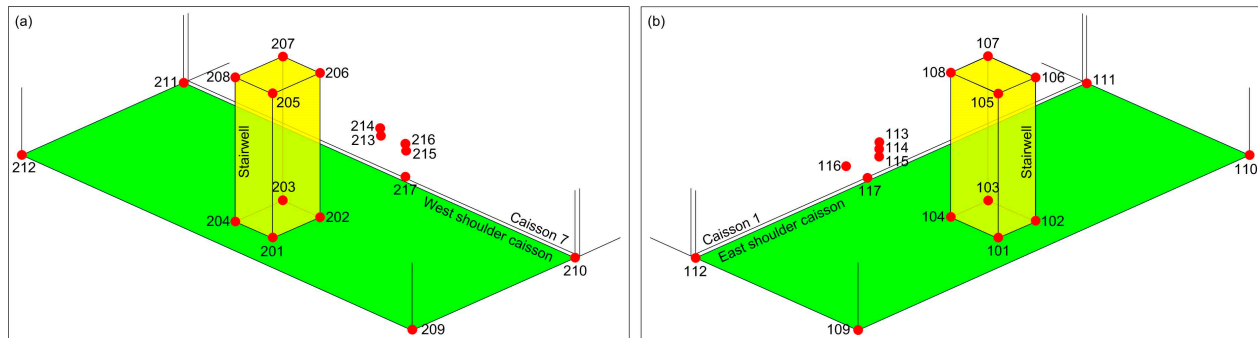


Figure 10. Location of the 17 points used in the calculation of the parameters for the transformation between the project/as-built and the survey reference systems for the west (a) and east (b) shoulder caissons: 101–108 are the corners of the east stairwell; 109–112 are the corners of the east shoulder caisson plate; 113–117 are points closed to the rubber joint of separation between the east shoulder and the first caissons of the barrier; 201–208 are the corners of the west stairwell; 209–212 are the corners of the west shoulder caisson plate; and 213–217 are points closed to the rubber joint of separation between the last and the west shoulder caissons and of the barrier.

In addition, for the east and west shoulder structures, five other points belonging to the shoulder and adjacent caissons in the edge area were available; these points, introduced to evaluate the separation between the two caissons, were used only to check the differences between the distance surveyed and those obtained from the processing.

The application of the Procrustean algorithm allowed to obtain the rotation and translation parameters with maximum residuals on the 17 used points of less than 2.5 cm, both for the east and west shoulder caissons. This value, the best-obtained result, is strongly influenced by the approximation of the real-built structures with respect to the designed elements.

The resulting parameters were then used to calculate the project/as-built coordinates of the new reference points fixed on the structures after the placement of the shoulder caissons on the seabed and measured in the survey reference system. In the next surveys, the 3D orientations of the caissons will be performed starting from these new reference points, with the same procedure applied to the other barriers.

Using data derived from the transformation, the distances between the shoulder and adjacent caissons were calculated both for the east and west structures and compared with the values surveyed (Table 4).

Table 4. Comparison between the distances of the separation shoulder—adjacent caissons calculated averaging the values at five points—and the surveyed data, both for the east and west structures.

Caissons	Calculated Distance (m)	Surveyed Distance (m)	Differences (m)
East shoulder caisson—Caisson 1	0.1890	0.1960	0.0070
Caisson 7—West shoulder caisson	0.1898	0.1947	0.0049

The obtained differences were in the order of few millimeters; this validation allowed to calculate a reliable value of the floodgate gap between the shoulder and the adjacent caissons, both for the east and west structures. Finally, the floodgate gap dimensions of 0.1825 m and 0.1866 m for the east and west elements, respectively, were estimated.

These values were integrated with those calculated from the topographic survey of the external and internal networks conducted on 21 March 2023, obtaining the complete orientation of the Treporti barrier. The temporal difference between the topographic survey of the networks and the TLS-stairwells surveys was less than six months and can be acceptable, since from the multi-temporal comparisons of the data acquired in the most recent period, the relative movements of the structures ended with the stabilization of the elements.

Additionally, it should be noted that with the performed method, the accuracy of floodgate gap detection using topographic measurements performed only in the tunnels and projected to the corners of the floodgates cannot be at the millimeter level, as reported in many comparable works [4,10]. In this way, all floodgate gaps of the Treporti barrier were calculated.

The validation of the obtained results was performed in the Treporti barrier using the drone-based SfM photogrammetric survey.

3.2. The SfM 3D Photogrammetric Model and the Floodgate Gaps Measurements

The photogrammetric processing of acquired drone-based imagery using Agisoft Metashape software version 1.8.4 provided a sparse point cloud from the alignment phase. CPs, used in the processing to georeference the data, and ChPs, used to validate the 3D model, provided RMSE values of 0.011 m and 0.016 m, respectively. Many other authors that worked in similar contexts obtained similar accuracies [3,49]. Subsequently, the dense cloud was extracted (Figure 11).

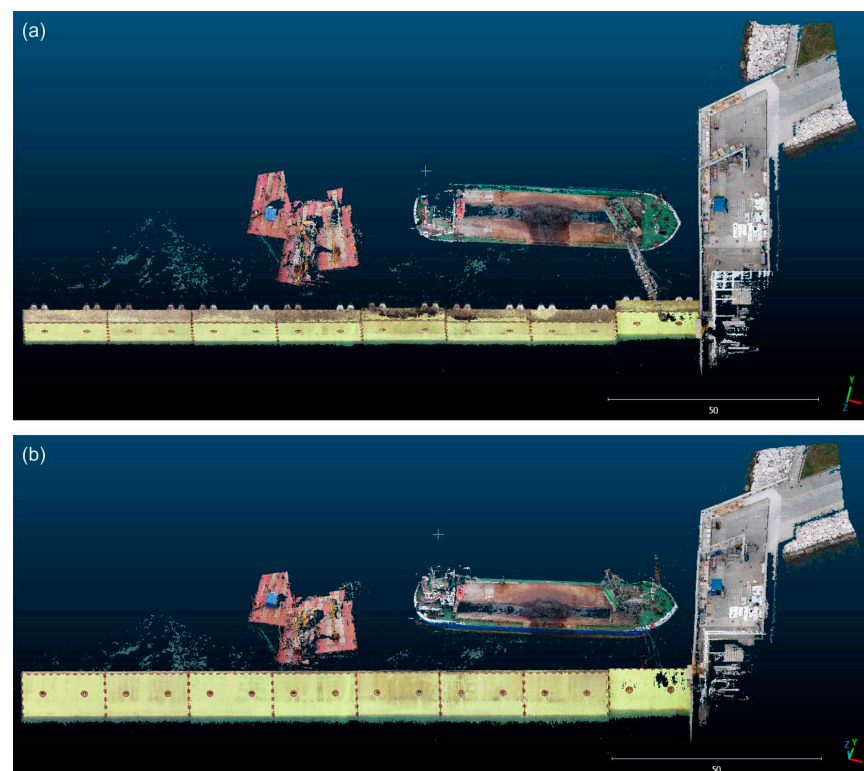


Figure 11. Dense 3D point cloud obtained via the SfM photogrammetric processing of drone-based imagery representing the system of the eight metallic raised floodgates and the emerged structures of the east shoulder caisson. Service boats for maintenance operations were also involved in the survey. The (a) thickness and (b) frontal faces of the yellow floodgates are shown.

Ten horizontal planes, starting from 1 m above the mean sea level (to avoid a fluctuation of the seawater) and up to the top of the raised metallic elements, were defined on the 3D model using Cyclone 3DR software. These planes intersected the model, generating ten horizontal sections used for the measurements of the floodgates and the gaps between the elements (Figure 12a). However, due to the noise on the 3D model caused by the subverticality of the raised floodgates, it was preferred to carry out other measurements by means of the ten sections obtained with vertical planes that intersected the top surfaces of the floodgates (on the thickness of the raised floodgates, Figure 12b). For each of the ten obtained vertical sections, an expert software operator measured the floodgate length and the gaps between the elements, from the emerged structures of the east shoulder to the eighth floodgate of the point cloud. These measurements were repeated for a second time for better statistical analysis. Finally, 20 measurements for each floodgate and gap were obtained; in this way, the results related to the longitudinal sizes (along the barrier) are provided in terms of mean and standard deviation values (Tables 5 and 6).

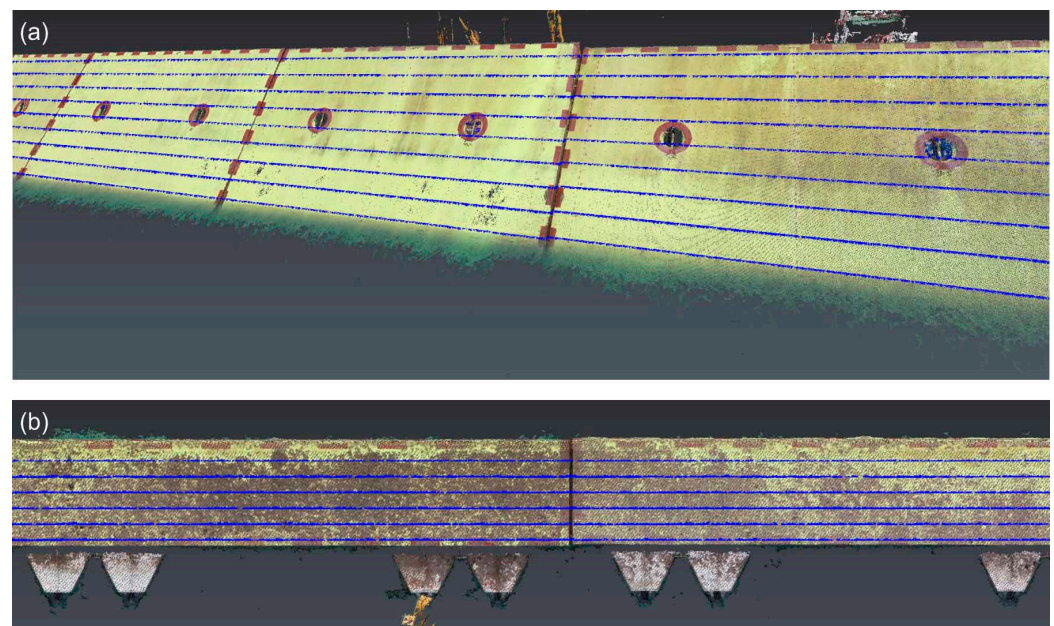


Figure 12. Trace of the intersection (in blue) between some horizontal (a) and vertical (b) planes with the 3D point cloud. Measurements of floodgate length and its gaps were more accurate using vertical planes.

Table 5. Maximum, minimum, mean, and standard deviation values of the 20 floodgate length measurements from the emerged structure of the east shoulder caisson to the eighth floodgate. In the last row, the comparisons between the designed values available from the project (19.88 m) and the measured mean values are reported.

Floodgates	1	2	3	4	5	6	7	8
Max (m)	18.887	19.907	19.920	19.894	19.894	19.921	19.902	19.884
Min (m)	19.833	19.883	19.863	19.859	19.868	19.881	19.850	19.831
Mean (m)	19.855	19.895	19.901	19.872	19.880	19.904	19.866	19.858
Standard deviation (m)	0.0148	0.0067	0.0138	0.0109	0.0088	0.0107	0.0145	0.0109
Designed values (m)	19.880	19.880	19.880	19.880	19.880	19.880	19.880	19.880
Comparison (m)	0.025	−0.015	−0.021	0.008	0.000	−0.024	0.014	0.022

The standard deviations of the 20 measurements, both for the floodgate length (Table 5) and gaps (Table 6), provided values up to 1.5 cm. These uncertainties are more than acceptable for floodgate gaps monitoring using this approach.

Table 6. Maximum, minimum, mean, and standard deviation values of the 20 floodgate gap measurements from the emerged structure of the east shoulder caisson (0 in the table) to the eighth floodgate. In the last row, the comparisons between the designed values available from the project and the measured mean values are reported.

Gaps Between Floodgates	0–1	1–2	2–3	3–4	4–5	5–6	6–7	7–8
Max (m)	0.195	0.175	0.139	0.237	0.158	0.136	0.217	0.139
Min (m)	0.169	0.124	0.094	0.202	0.116	0.112	0.189	0.118
Mean (m)	0.184	0.142	0.124	0.218	0.137	0.125	0.203	0.132
Standard deviation (m)	0.009	0.014	0.012	0.008	0.012	0.008	0.008	0.005
Designed values (m)	0.170	0.120	0.120	0.200	0.120	0.120	0.200	0.120
Comparison (m)	−0.014	−0.022	−0.004	−0.018	−0.017	−0.005	−0.003	−0.012

Since three floodgates are located in each caisson, with the drone-based photogrammetric survey, the following were estimated: (i) the length of each floodgate (Table 5); (ii) the gaps between floodgates placed in the same caisson (1–2, 2–3, 4–5, 5–6, 7–8); and (iii) the gaps between floodgates belonging to adjacent caissons (0–1, 3–4, 6–7) (Table 6). These values, compared with the designed values available from the projects, provided differences that can be due to the following: (i) errors of the SfM photogrammetric model, including the uncertainties of the operator in the manual measurements; (ii) the imperfect construction and installation of the structures (including the tolerance values of the metallic constructions); and (iii) the real relative deformations (floodgate gaps 0–1, 3–4, 6–7 between different caissons) that occurred in the time span between the construction of the system and the drone-based SfM photogrammetric survey. The latter estimation showed (Table 6) that the obtained differences between the designed values and the measured floodgate gaps are of the same order of magnitude for both the floodgates belonging to the same caisson and the floodgates belonging to adjacent caissons, which indicates no significant relative deformations. Considering all these factors, the maximum differences of 2.5 cm, in agreement with the values reported by de Sousa Mello et al. [28] and Varbla et al. [30], can be acceptable in guaranteeing the correct operational functionality of the system.

The floodgate gaps measured between the metallic elements belonging to the adjacent caissons were also compared with the values calculated on the basis of topographic surveys and TLS acquisitions, performed in the same period (Figure 13).

In this way, the data acquired with the total station in the tunnels and laser scanner in the stairwell can be validated. Table 7 provides the results of the comparison.

Table 7. Floodgate gap values between the metallic elements belonging to adjacent caissons (0 representing the emerged structures in the east shoulder caisson), obtained from the topographic surveys in the tunnels integrated with the TLS of the stairwell and the measurements performed on the 3D SfM photogrammetric model.

Survey Technique	Floodgate Gaps		
	0–1	3–4	6–7
Topography—TLS (m)	0.183	0.213	0.187
SfM photogrammetry (m)	0.184	0.218	0.203
Differences (m)	−0.001	−0.005	−0.016

Maximum differences of 1.6 cm are in agreement with the expected results in terms of final accuracies using drone-based SfM photogrammetry [28,30], and the floodgate gaps calculated from topographic—TLS surveys performed in the tunnels—stairwells. In this way, the obtained differences allowed the validation of the topographic measurements, TLS acquisitions, and data processing based on the Procrustean algorithm for the estimation of floodgate gaps.

Based on these data, and those obtained in the other barriers with the topographic approach, currently there are no significant relative deformations of both the floodgate

gaps and the rubber joints of the MOSE system. For these reasons, the full operability of the MOSE system was verified because the floodgates can be raised without the risk of collisions between the metallic elements, and the tunnels are well protected from flooding by the rubber joints, since their operating field has not reached the threshold values.

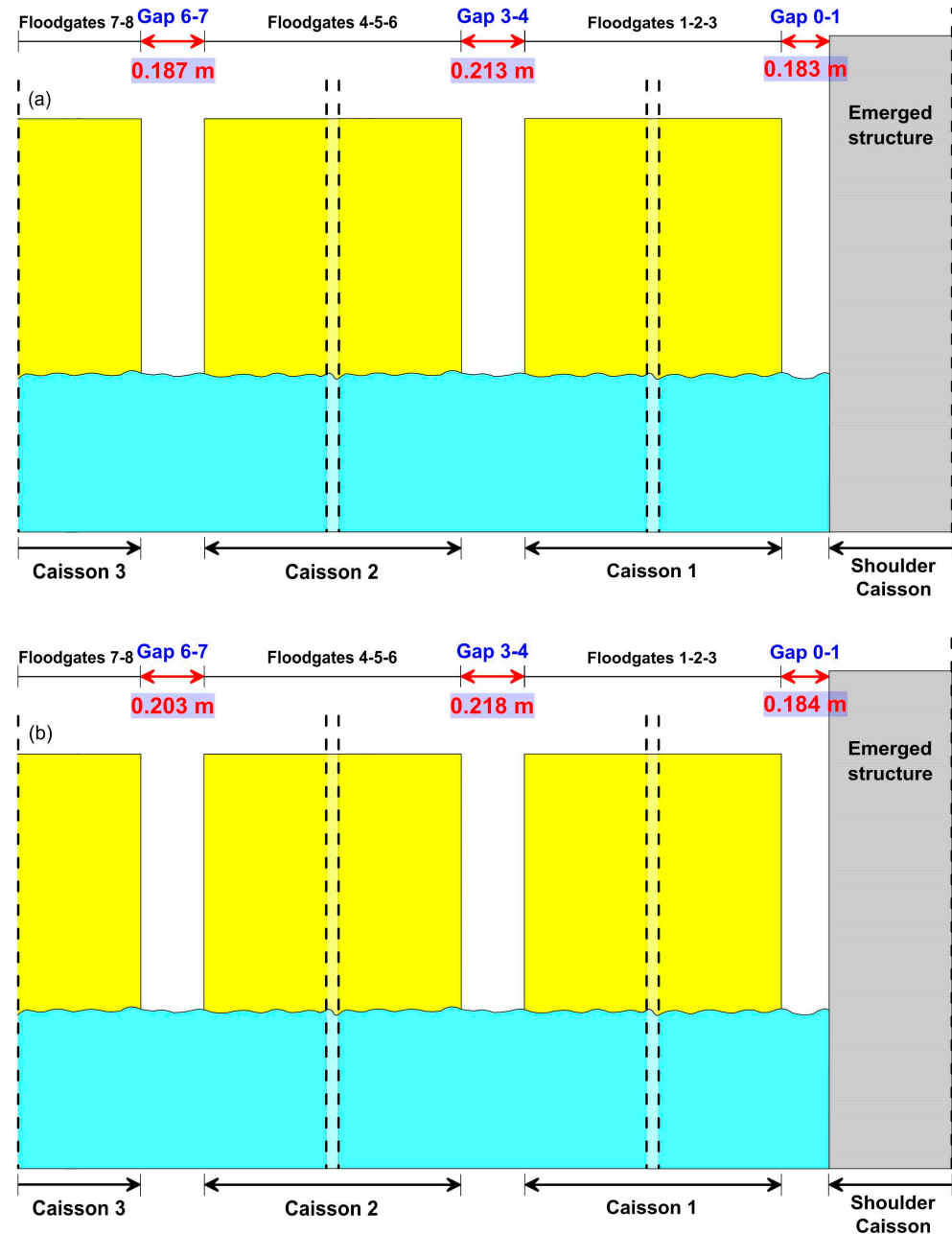


Figure 13. Final results of floodgate gaps between the metallic elements belonging to the adjacent caissons in the Treporti barrier obtained on the basis of topographic surveys and TLS acquisitions (a) and the measurements performed on the 3D SfM photogrammetric model (b).

From a methodological point of view, this study shows the advantages and limitations of the SfM and topographic (measurements using total stations) approaches in the definitions of floodgate gaps. While the total station could be considered the best device for the acquisition of high-accuracy data in direct single measurements, it needs good stationing possibilities, intervisibility between points, and a proper environment. The complexity of the MOSE system does not always allow complete and easy accessibility to all parts of the structure: the topographic measurements of the submerged elements can be performed

only in the tunnels, and the obtained measures need to be projected to the corners of the floodgates, losing the original millimeter accuracy. In this regard, aerial photogrammetry is an efficient technique that overcomes some logistic issues and allows to measure, through the 3D model, the floodgate gaps, which are not reachable with a total station. However, the accuracy of SfM, at the centimeter level, and the need for the stability of the raised floodgates during the acquisition phase, pose evident limitations.

Considering all these aspects, the co-validation between datasets is crucial to estimate the reliability of the results. It is based on the comparison of data that come from independent measurements, processing, and statistical analysis, in order to obtain a proper final evaluation.

The co-validation of the data from these different approaches turned out to be an adequate solution to be implemented in other similar cases, where the application of the most suitable technique is not always possible, and when topographic measurements and 3D surveys could be integrated, exploiting the best peculiarities of each technique.

3.3. Future Developments

The 3D survey and topographic monitoring presented in this work represent a crucial activity in the study of the deformations of the MOSE system and how its operation could affect the functionality of mobile elements and fixed structures. Assuming the results obtained in this work that compare project values with current real measured values, a constant control turned out to be necessary to guarantee high standards for this important feat of engineering that protects the city of Venice.

Above all, rubber joints and floodgate gaps require continuous monitoring. For this purpose, the relative movements of the caissons must be measured, integrating different sensors in an automatic monitoring system. The ongoing activities concern the installation of the following: (i) 36 continuous GNSS (CGNSS) stations (located on corners of the emerged structures of the shoulder caissons together with a reference station for each barrier); (ii) eight strain gauges in the main tunnel of the four barriers; (iii) 70 inclinometers (one for each submerged caisson) located in the secondary tunnel of the four barriers; and (iv) joint measuring devices located in the separations between the different caissons along the main tunnel. The integration between the different sensors allows the continuous, automatic 3D spatial positioning calculation of each caisson with the continuous rubber joints and floodgate gaps deformation monitoring during all the operational phases of the system. However, the topographic measurements of networks will continue to be carried out for the calibration of the system and the validation of automatic monitoring.

4. Conclusions

In this work, topographic measurements using total stations and levels, a drone-based SfM photogrammetric survey, and TLS acquisitions were used for the relative deformations monitoring of the floodgate gaps and the rubber joints of the MOSE system, the civil infrastructure that protects Venice and its lagoon from high waters.

The TLS technique, together with the Procrustean algorithm, allowed to solve the problem related to the definition of the shoulder caissons 3D orientation in the Treporti barrier, as we obtained residuals of transformation between the project and the survey reference systems of less than 2.5 cm. These values are more than acceptable taking into account the approximation of the concrete real-built structures.

The topographic measurements of external and internal networks, integrated with TLS acquisitions, allowed to obtain crucial data in the estimation of the floodgate gaps, since the validation using a drone-based SfM photogrammetric survey in the Treporti barrier provided maximum differences of 1.6 cm.

The drone-based SfM photogrammetric survey demonstrated its usefulness not only for the validation of the topographic and TLS estimations. Given the achieved accuracies, in the order of a few centimeters, and the easy and flexible application of this technique, the frequent repetition of these surveys is recommended, both for the direct floodgate

gap deformation monitoring and the evaluation of the degradation status of the metallic elements. These activities can be programmed when the floodgates are raised during maintenance phases, being careful with the stability of the floodgates during the image acquisitions (the absence of wind and wave motion, reduction of the shadow areas, etc.) to guarantee the final accuracies.

The analysis developed in this study allowed the following: (i) evaluate the data uncertainties of the used instruments and methodologies; (ii) verify the usefulness of the applied techniques and validate the methods implemented for the monitoring activities with obtained accuracies at the centimeter-level; (iii) recommend the integration of the techniques and methods described in this work for the deformation monitoring of similar infrastructures in similar contexts; and (iv) establish the general stability achieved by the MOSE system in terms of relative deformations.

Finally, this work has demonstrated the validity of the proposed procedures based on the integration between different methods to generate an efficient deformation monitoring system of the MOSE infrastructure. Acquired and processed data were crucial to ensure the efficiency and operability of the lagoon and the city of Venice protection system from high waters, which in recent years, have caused extensive environmental, economic, and structural damages. Furthermore, the study provided key points for new deformation monitoring activities and can be applied in similar cases when submerged/emerged and/or fixed/mobile structures are used to protect wide territories against flooding from sea and river waters.

Author Contributions: Conceptualization, M.F.; methodology, M.F. and M.M.; software, M.F. and M.M.; validation, M.F. and M.M.; formal analysis, M.F. and M.M.; investigation, M.F.; resources, M.F.; data curation, M.F.; writing—original draft preparation, M.F.; writing—review and editing, M.F. and M.M.; visualization, M.F. and M.M.; supervision, M.F.; project administration, M.F. All authors have read and agreed to the published version of the manuscript.

Funding: This research received no external funding.

Data Availability Statement: Restrictions apply to the availability of these data. Data were obtained from Consorzio Venezia Nuova.

Acknowledgments: The authors would like to thank the “Ministero delle Infrastrutture e dei Trasporti—Provveditorato Interregionale per le Opere Pubbliche del Veneto—Trentino Alto Adige—Friuli Venezia Giulia”, Consorzio Venezia Nuova, and Irene D’Urso, MSCE (Master of Science in Civil Engineering) and Massimo Pravato of the Thetis SpA; the “Laboratory of Geomatics and Surveying” staff of the University of Padova.

Conflicts of Interest: The authors declare no conflicts of interest.

References

1. Yang, H.; Xu, X. Structure monitoring and deformation analysis of tunnel structure. *Compos. Struct.* **2021**, *276*, 114565. [\[CrossRef\]](#)
2. Moyano, J.; Nieto-Julián, J.E.; Bienvenido-Huertas, D.; Marín-García, D. Validation of Close-Range Photogrammetry for Architectural and Archaeological Heritage: Analysis of Point Density and 3D Mesh Geometry. *Remote Sens.* **2020**, *12*, 3571. [\[CrossRef\]](#)
3. Capolupo, A. Accuracy Assessment of Cultural Heritage Models Extracting 3D Point Cloud Geometric Features with RPAS SfM-MVS and TLS Techniques. *Drones* **2021**, *5*, 145. [\[CrossRef\]](#)
4. Omidalizarandi, M.; Kargoll, B.; Paffenholz, J.-A.; Neumann, I. Accurate vision-based displacement and vibration analysis of bridge structures by means of an image-assisted total station. *Adv. Mech. Eng.* **2018**, *10*, 6. [\[CrossRef\]](#)
5. Pepe, M.; Costantino, D.; Alfio, V.S. Topographic Measurements and Statistical Analysis in Static Load Testing of Railway Bridge Piers. *Infrastructures* **2024**, *9*, 4. [\[CrossRef\]](#)
6. Capra, A.; Bertacchini, E.; Castagnetti, C.; Rivola, R.; Dubbini, M. Recent approaches in geodesy and geomatics for structures monitoring. *Rend. Lincei* **2015**, *26*, 53–61. [\[CrossRef\]](#)
7. Dardanelli, G.; Allegra, M.; Giammarresi, V.; Lo Brutto, M.; Pipitone, C.; Baiocchi, V. Geomatic methodologies for the study of Teatro Massimo in Palermo (Italy). In Proceedings of the International Archives of the Photogrammetry, Remote Sensing and Spatial Information Sciences, Florence, Italy, 22–24 May 2017; Volume XLII-5/W1, pp. 475–480. [\[CrossRef\]](#)
8. Yuwono, B.D.; Prasetyo, Y. Analysis Deformation Monitoring Techniques Using GNSS Survey and Terrestrial Survey (Case Studi: Diponegoro University Dam, Semarang, Indonesia). *IOP Conf. Ser. Earth Environ. Sci.* **2018**, *313*, 012045. [\[CrossRef\]](#)

9. Magnaval, G.; Colette, T.; Boumeshal, M. Combination of Total Station and GNSS for the Monitoring of Civil Infrastructures in Dense Urban Areas. In *Proceedings of the 10th European Workshop on Structural Health Monitoring, EWSHM, Palermo, Italy, 4–7 July 2022, Code 279319*; Lecture Notes in Civil Engineering; Springer: Berlin/Heidelberg, Germany, 2023; Volume 254, pp. 51–58.
10. Selvakumaran, S.; Rossi, C.; Marinoni, A.; Webb, G.; Bennetts, J.; Barton, E.; Plank, S.; Middleton, C. Combined InSAR and Terrestrial Structural Monitoring of Bridges. *IEEE Trans. Geosci. Remote Sens.* **2020**, *58*, 7141–7153. [\[CrossRef\]](#)
11. Debus, P.; Rodehorst, V. Multi-scale Flight Path Planning for UAS Building Inspection. In *Proceedings of the 18th International Conference on Computing in Civil and Building Engineering, Sao Paulo, Brazil, 18–20 August 2020*; Lecture Notes in Civil Engineering; Springer: Berlin/Heidelberg, Germany, 2021; Volume 98, pp. 1069–1085. [\[CrossRef\]](#)
12. Galarreta, J.F.; Kerle, N.; Gerke, M. UAV-based urban structural damage assessment using object-based image analysis and semantic reasoning. *Nat. Hazards Earth Syst. Sci.* **2015**, *15*, 1087–1101. [\[CrossRef\]](#)
13. Hallermann, N.; Morgenthal, G.; Rodehorst, V. Unmanned aerial systems (UAS)—Case studies of vision-based monitoring of ageing structures. In *Proceedings of the International Symposium Non-Destructive Testing in Civil Engineering, Berlin, Germany, 15–17 September 2015*.
14. Sankarasrinivasan, S.; Balasubramanian, E.; Karthik, K.; Chandrasekar, U.; Gupta, R. Health monitoring of civil structures with integrated UAV and image processing system. *Procedia Comput. Sci.* **2015**, *54*, 508–515. [\[CrossRef\]](#)
15. Ellenberg, A.; Branco, L.; Krick, A.; Bartoli, I.; Kontsos, A. Use of unmanned aerial vehicle for quantitative infrastructure evaluation. *J. Infrastruct. Syst.* **2015**, *21*, 04014054. [\[CrossRef\]](#)
16. Kim, H.; Lee, J.; Ahn, E.; Cho, S.; Shin, M.; Sim, S.H. Concrete crack identification using a UAV incorporating hybrid image processing. *Sensors* **2017**, *17*, 2052. [\[CrossRef\]](#) [\[PubMed\]](#)
17. Lei, B.; Wang, N.; Xu, P.; Song, G. New crack detection method for bridge inspection using UAV incorporating image processing. *J. Aerosp. Eng.* **2018**, *31*, 04018058. [\[CrossRef\]](#)
18. Duque, L.; Seo, J.; Wacker, J. Bridge deterioration quantification protocol using UAV. *J. Bridge Eng.* **2018**, *23*, 04018080. [\[CrossRef\]](#)
19. Rashidi, M.; Samali, B. Health monitoring of bridges using rpas. *Lect. Notes Civ. Eng.* **2021**, *101*, 209–218. [\[CrossRef\]](#)
20. Germanese, D.; Leone, G.R.; Moroni, D.; Pascali, M.A.; Tampucci, M. Long-term monitoring of crack patterns in historic structures using UAVs and planar markers: A preliminary study. *J. Imaging* **2018**, *4*, 99. [\[CrossRef\]](#)
21. Paglinawan, A.C.; Cruz, F.R.G.; Casi, N.D.; Ingatan, P.A.B.; Karganilla, A.B.C.; Moster, G.V.G. Crack Detection Using Multiple Image Processing for Unmanned Aerial Monitoring of Concrete Structure. In *Proceedings of the IEEE Region 10 Annual International Conference, Jeju, Republic of Korea, 28–31 October 2018*; pp. 2534–2538. [\[CrossRef\]](#)
22. Kalaitzakis, M.; Kattil, S.R.; Vitzilaios, N.; Rizos, D.; Sutton, M. Dynamic structural health monitoring using a DIC-enabled drone. In *Proceedings of the International Conference on Unmanned Aircraft Systems, ICUAS 2019, Atlanta, GE, USA, 11–14 June 2019*; pp. 321–327. [\[CrossRef\]](#)
23. Tian, Y.; Chen, C.; Sagoe-Crentsil, K.; Zhang, J.; Duan, W. Intelligent robotic systems for structural health monitoring: Applications and future trends. *Autom. Constr.* **2022**, *139*, 104273. [\[CrossRef\]](#)
24. Lee, S.B.; Song, M.; Kim, S.; Won, J.H. Change monitoring at expressway infrastructure construction sites using drone. *Sens. Mater.* **2020**, *32*, 3923–3933. [\[CrossRef\]](#)
25. Yi, W.; Sutrisna, M. Drone scheduling for construction site surveillance. *Comput.-Aided Civ. Infrastruct. Eng.* **2021**, *36*, 3–13. [\[CrossRef\]](#)
26. Casierra, C.B.G.; Sánchez, C.G.C.; García, J.F.C.; Rivera, F.M.L. Methodology for Infrastructure Site Monitoring using Unmanned Aerial Vehicles (UAVs). *Int. J. Adv. Comput. Sci. Appl.* **2022**, *13*, 340–348. [\[CrossRef\]](#)
27. Cuypers, S.; De Winter, H.; Bassier, M.; Vergauwen, M. Planimetric rail positioning using UAV photogrammetry: Towards automated and safe railway infrastructure monitoring. In *Proceedings of the International Archives of the Photogrammetry, Remote Sensing and Spatial Information Sciences—ISPRS Archives, Cairo, Egypt, 2–7 September 2023*; Volume 48, pp. 589–596.
28. De Sousa Mello, C.C.; Salim, D.H.C.; Simões, G.F. UAV-based landfill operation monitoring: A year of volume and topographic measurements. *Waste Manag.* **2022**, *137*, 253–263. [\[CrossRef\]](#) [\[PubMed\]](#)
29. Fabris, M.; Balin, M.; Monego, M. High-Resolution Real-Time Coastline Detection Using GNSS RTK, Optical, and Thermal SfM Photogrammetric Data in the Po River Delta, Italy. *Remote Sens.* **2023**, *15*, 5354. [\[CrossRef\]](#)
30. Varbla, S.; Ellmann, A.; Puust, R. Centimetre-range deformations of built environment revealed by drone-based photogrammetry. *Autom. Constr.* **2021**, *128*, 103787. [\[CrossRef\]](#)
31. Zrinjski, M.; Tupek, A.; Barković, Đ.; Polović, A. Industrial Masonry Chimney Geometry Analysis: A Total Station Based Evaluation of the Unmanned Aerial System Photogrammetry Approach. *Sensors* **2021**, *21*, 6265. [\[CrossRef\]](#) [\[PubMed\]](#)
32. Adi, W.T.; Aghastya, A.; Prihatanto, R.; Agustriana, T.M. Measurement of railway ballast deficiency using UAV drone and total station by graphical, statistical, and volume comparison. In *Proceedings of the International Conference on Mechanical Engineering for Emerging Technologies (ICOMEET 2021), Padang, Indonesia, 3–4 November 2021*; Volume 2592, p. 050013. [\[CrossRef\]](#)
33. Tomasicchio, G.R.; Salvadori, G.; Lusito, L.; Francone, A.; Saponieri, A.; Leone, E.; De Bartolo, S. A Statistical Analysis of the Occurrences of Critical Waves and Water Levels for the Management of the Operativity of the MoSE System in the Venice Lagoon. *Stoch. Environ. Res. Risk Assess.* **2022**, *36*, 2549–2560. [\[CrossRef\]](#)
34. Casasso, A.; Di Molfetta, A.; Sethi, R. Groundwater monitoring at a building site of the tidal flood protection system “MOSE” in the Lagoon of Venice, Italy. *Environ. Earth Sci.* **2015**, *73*, 2397–2408. [\[CrossRef\]](#)

35. Cavallaro, L.; Iuppa, C.; Foti, E. Effect of Partial Use of Venice Flood Barriers. *J. Mar. Sci. Eng.* **2017**, *5*, 58. [CrossRef]
36. Umgiesser, G. The impact of operating the mobile barriers in Venice (MOSE) under climate change. *J. Nat. Conserv.* **2020**, *54*, 125783. [CrossRef]
37. Gower, J.; Barale, V. The Rising Concern for Sea Level Rise: Altimeter Record and Geo-Engineering Debate. *Remote Sens.* **2024**, *16*, 262. [CrossRef]
38. Wang, G.; Liu, Y.; Hu, Z.; Zhang, G.; Liu, J.; Lyu, Y.; Gu, Y.; Huang, X.; Zhang, Q.; Liu, L. Flood Risk Assessment of Subway Systems in Metropolitan Areas under Land Subsidence Scenario: A Case Study of Beijing. *Remote Sens.* **2021**, *13*, 637. [CrossRef]
39. Gower, J.C. Generalized procrustes analysis. *Psychometrika* **1975**, *40*, 33–51. [CrossRef]
40. Goodall, C. Procrustes methods in the statistical analysis of shape. *J. R. Stat. Soc. Ser. B Methodol.* **1991**, *53*, 285–339. [CrossRef]
41. Agisoft LLC. *Agisoft Metashape User Manual*; Professional Edition, Version 1.8; Agisoft LLC: St. Petersburg, Russia, 2022.
42. Agisoft LLC. *Metashape Python Reference*, Release 1.8.2; Agisoft LLC: St. Petersburg, Russia, 2022.
43. Monego, M.; Achilli, V.; Fabris, M.; Menin, A. 3-D Survey of Rocky Structures: The Dolomitic Spire of the Gusela del Vescovà. In *Proceedings of the 1st International Workshop in Memory of Professor Raffaele Santamaria on R3 in Geomatics: Research, Results and Review, R3GEO 2019, Naples, Italy, 10–11 October 2019*; Communications in Computer and Information Science 2020; Springer: Berlin/Heidelberg, Germany; Volume 1246, pp. 211–228.
44. Fabris, M.; Fontana Granotto, P.; Monego, M. Expeditionary Low-Cost SfM Photogrammetry and a TLS Survey for the Structural Analysis of Illasi Castle (Italy). *Drones* **2023**, *7*, 101. [CrossRef]
45. Leica Geosystems. Available online: <https://leica-geosystems.com/products/laser-scanners/software/leica-cyclone/leica-cyclone-register-360> (accessed on 28 July 2023).
46. Pieraccini, M.; Dei, D.; Betti, M.; Bartoli, G.; Tucci, G.; Guardini, N. Dynamic identification of historic masonry towers through an expeditionary and no-contact approach: Application to the “Torre del Mangia” in Siena (Italy). *J. Cult. Herit.* **2014**, *15*, 275–282. [CrossRef]
47. Monego, M.; Fabris, M.; Menin, A.; Achilli, V. 3-D Survey applied to industrial archaeology by tls methodology. In *Proceedings of the International Archives of the Photogrammetry, Remote Sensing and Spatial Information Sciences*, Florence, Italy, 22–24 May 2017; Volume XLII-5/W1, pp. 449–455. [CrossRef]
48. CloudCompare (Version 2.12 Alpha). Available online: <http://www.cloudcompare.org/> (accessed on 15 February 2024).
49. Sanseverino, A.; Messina, B.; Limongiello, M.; Guida, C.G. An HBIM Methodology for the Accurate and Georeferenced Reconstruction of Urban Contexts Surveyed by UAV: The Case of the Castle of Charles V. *Remote Sens.* **2022**, *14*, 3688. [CrossRef]

Disclaimer/Publisher’s Note: The statements, opinions and data contained in all publications are solely those of the individual author(s) and contributor(s) and not of MDPI and/or the editor(s). MDPI and/or the editor(s) disclaim responsibility for any injury to people or property resulting from any ideas, methods, instructions or products referred to in the content.